

Received December 22, 2016, accepted January 1, 2017, date of publication January 4, 2017, date of current version January 27, 2017.

Digital Object Identifier 10.1109/ACCESS.2017.2647851

Hybrid Control of a Vision-Guided Robot Arm by EOG, EMG, EEG Biosignals and Head Movement Acquired via a Consumer-Grade Wearable Device

LUDOVICO MINATI^{1,2,3}, (Senior Member, IEEE), NATSUE YOSHIMURA⁴,
AND YASUHARU KOIKE⁴

¹Tokyo Tech World Research Hub Initiative, Institute of Innovative Research - Tokyo Institute of Technology, Yokohama 226-8503, Japan

²Complex Systems Theory Department, Institute of Nuclear Physics - Polish Academy of Sciences, Kraków 31-342, Poland

³Center for Mind/Brain Sciences, University of Trento, Trento 38123, Italy

⁴FIRST, Institute of Innovative Research - Tokyo Institute of Technology, Yokohama, Japan

Corresponding author: L. Minati (ludovico.minati@ifj.edu.pl)

This work was supported in part by JSPS under Grant KAKENHI 26112004 and Grant KAKENHI 15H01659 and in part by the Center of Innovation Program from the Japan Science and Technology Agency, JST. Realization of the robot arm hardware was personally funded by L. Minati. The authors have no relationships and have never been in contact with InteraXon Inc., Toronto, Canada. L. Minati gratefully acknowledges funding by the World Research Hub Initiative, Institute of Innovative Research, Tokyo Institute of Technology, Tokyo, Japan.

ABSTRACT Simultaneous acquisition of electrooculogram, jaw electromyogram, electroencephalogram, and head movement via consumer-grade wearable devices has become possible. Such devices offer new opportunities to deploy practical biosignal-based interfaces for assistive robots; however, they also pose challenges related to the available signals and their characteristics. In this proof-of-concept study, we demonstrate the possibility of successful control of a 5 + 1 degrees-of-freedom robot arm based on a consumer wireless headband in the form of four control modes predicated on distinct signal combinations. We propose a control approach hybrid at two levels, which seeks a compromise between robot controllability and maintaining the user goal rather than being process-focused. First, robot arm steering combines discrete and proportional aspects. Second, after the robot has been steered toward the approximate target direction, a sparse approach is followed and the user only needs to issue a single command, after which steering adjustment and grasping are performed automatically under stereoscopic vision guidance. We present in detail the associated algorithms, whose implementation is publicly available. Within this framework, we also demonstrate the control of arm posture and grasping force based, respectively, on object visual features and user input. We regard the interface proposed herein as a viable blueprint for future work on controlling wheelchair-mounted and meal-assisting robot arms.

INDEX TERMS Accelerometer, assistive robotics, brain-computer interface (BCI), brain-machine interface (BMI), electrooculogram (EOG), electroencephalogram (EEG), electromyogram (EMG), event-related desynchronization/synchronization (ERD/ERS), grasping force, human-machine interface (HMI), meal-assisting robot, stereoscopic vision, wheelchair-mounted robot arm.

I. INTRODUCTION

Assistive robotics aims to improve quality of life and reduce caregiver dependence for patients whose motor functions have been impaired, e.g., by traumatic, vascular and neoplastic lesions, motor neuron and other neurological diseases; it also aims to enhance rehabilitation when function may be at least partially regained. Applied research has yielded, e.g., effective exoskeletons, wheelchair-mounted robotic manipulators for grasping and performing basic operations using everyday-life objects, and meal-assisting

tabletop robots [1], [2]. A substantial challenge in this area is to develop effective human-machine interfaces and paradigms for robot control, with the available technologies differing substantially in their residual motor function requirements, command throughput, ease of use, technical complexity and cost. At the bottom end of the spectrum, joystick (or micro-switch) control is suitable mainly for patients with at least partially preserved hand function (e.g., as after hemispheric stroke), being inexpensive and highly effective for driving, e.g., motorized wheelchairs and

assistive arms [3], [4]; gesture-based control via low-cost camera systems is also emerging as a suitable alternative, posing less stringent requirements on upper limb and head movement capability [5], [6]. Highly accurate control of assistive devices has repeatedly been demonstrated based on superficially-recorded face-muscle electromyographic (EMG) and/or electrooculographic (EOG) signals; although harvesting information from these signals is generally more expensive and technically-demanding compared to micro-switch and camera-based interfaces, at a minimum, it only requires integrity of the cranial nerves function, which is generally preserved in patients with spinal lesions [7]–[12]. At the top end of the spectrum with respect to complexity and cost, brain-computer interfaces (BCI) and brain-machine interfaces (BMI) rely on electroencephalographic (EEG) signals, thus bypassing neuromuscular control entirely and being viable even in the presence of profound or total motor impairment, such as in the case of motor neuron diseases and brainstem lesions [13]–[16].

Research on BCI/BMI systems has been propelled by the achievement of ever-increasing raw bit rates, implementation of practically-useable speller and graphical-use interface control applications, and reconstruction of detailed muscle activity from surface EEG signals [17]–[20]. However, to date the translation of such successes into commercially-available products impacting clinical reality has been considerably hindered by practical factors: channel count, positioning and signal quality requirements, together with technical complexity and computational load; multiple reviews of this area therefore underline the need for greater focus on usability outside research settings, cost and availability [14], [15], [21], [22]. It is generally agreed upon that ongoing development of dry-electrode and ultrahigh-impedance technology will eventually lower BCI/BMI deployment barriers, stemming from the need for high-density, high-quality EEG acquisition [23], [24]. However, several experimental studies have concluded that at the present time, adopting a multi-modal approach in practical applications of assistive robot control has substantial benefits, as command decoding can be simplified and accelerated by considering EOG and EMG signals, when these are available [16], [25]–[27]. Following this trend, many low-cost, small-size wearable devices suitable for acquiring EOG and EMG, alongside a limited number of EEG channels, have recently been developed [28]–[33].

Another challenge in assistive robotics is the frequent requirement to control large numbers of degrees-of-freedom. When bio-signal acquisition from multiple viable muscle bundles, nerve stumps or even the motor cortex itself is feasible, direct patient control of all individual robot axes offers the highest grade of flexibility and is particularly applicable to driving exoskeletons, prosthetic hands or anthropomorphic robot arms [7], [34]. Moreover, high-precision and proportional control of single axes have been consistently demonstrated based on surface EMG and even EOG [8], [35]–[37]. Yet, many practical applications of assistive robotics would

benefit from control of complex mechanics based on a heavily constrained set of bio-signals acquired non-invasively, while allowing the user to focus on their goal rather than on kinematics. This need has driven recourse to either degrees-of-freedom reduction approaches, namely, linking axes via pre-determined relationships or postures, or “sparse” control schemes, wherein the user selects and activates pre-established motor sequences via “high-level” commands with or without the support of a graphical user interface [25], [33], [38]–[42]. Such approach has proven particularly effective when combined with computer vision systems implementing object recognition and partially-autonomous guidance, which can drastically simplify and accelerate the performance of object manipulation tasks using robotic arms and even humanoid robots [5], [42]–[46].

In this proof-of-concept study, we provide a blueprint for control of a $5 + 1$ degrees-of-freedom robot based on an inexpensive, consumer-grade wearable device capable of recording a combination of head movement, EOG, EMG and EEG signals. We propose a hybrid control approach, wherein steering of the robot arm is proportionally controlled directly by the participant and guidance by a stereoscopic vision system control implements automated reaching toward and grasping of a target in response to a single trigger command. We demonstrate and preliminarily compare four control modes attainable with data from this device. We exemplify grasping force control based on participant input and arm posture selection based on object visual properties. All ongoing signal analysis and control algorithms are described in detail, and the corresponding source code is publicly available.

II. METHODS

A. EXPERIMENTAL TASK

To demonstrate the viability of the control architecture and signal analysis algorithms described below, an experimental task was devised, requiring the participant to sort colored pawns into two cups depending on color: red and green to the left and right cup, respectively. The cylindrical pawns, having a diameter of 12 mm and height of 20 mm, were laid out in front of the robot and presented separately in 3 pre-established groups of 6 each (Fig. 1a). Half of the pawns per color were made of steel (weight: 18 g) and thus required application of a strong force for successful grasping; the other half needed to be grasped with very light force, as they were made of felt (weight <1 g) and contained a roll of double-sided tape, which would otherwise collapse and stick, revealing the application of excessive force (Fig. 1b). Additionally, the requirement was imposed that the red pawns should be picked-up with sideways posture, while the green ones, with straight posture (Fig. 1c). This task was similar to that utilized in a previous study on robot arm control via fMRI; however, it posed additional requirements on force and posture; as such, although elementary in concept, it necessitated fine control of all robot axes for



FIGURE 1. Experimental setup. a) Robot arm having 5 + 1 degrees-of-freedom (base rotation, shoulder, elbow, wrist, wrist rotation plus gripper), equipped with stereoscopic vision and gripper force sensors. The participant controlled it aiming to move the red and green pawns into the cups located respectively on the left and right sides. The solid (steel) and hollow (felt) pawns required, respectively, application of high and low grasping force. b) For demonstrating grasping force control by the participant, the felt pawns contained a circle of double-sided tape collapsing upon application of excessive force. c) Arm posture was selected automatically depending on pawn color. d) Frame-series depicting a representative grasping sequence.

successful performance and embodied the bases necessary for driving an assistive arm able to manipulate heterogeneous targets [45].

B. DATA ACQUISITION AND CONTROL MODES

All signals were digitized through a wearable device marketed primarily as a meditation aid (muse 2014; InteraXon

Inc., Toronto, Canada), which streamed polygraphic and head movement data via a Bluetooth “RFCOMM” link; its end-user price was approximately 1-2% of typical high-end EEG systems prevalent in current BCI/BMI research, rendering it, in principle, well-suitable for low-cost machine control interfaces. The device consisted of a headband encapsulating silver electrodes at the *Fpz* (recording reference), *AF7* and *AF8* sites and supra-auricular conductive rubber electrodes at *A1* and *A2* (approximate corresponding 10/20 system locations); it also included an active reference system, inputs for two additional cup electrodes, located at the *Pz* and *Fz* sites (only used in mode 4, as detailed below), and a 3-axis accelerometer (Fig. 2). Electrical bio-signals and accelerations were streamed, respectively, at 16-bit 500 Hz and 10-bit 50 Hz, with the corresponding signals parsed for command recognition at 10 Hz and 5 Hz. No part of the system described below is specifically dependent on usage of the “muse” device for data acquisition.

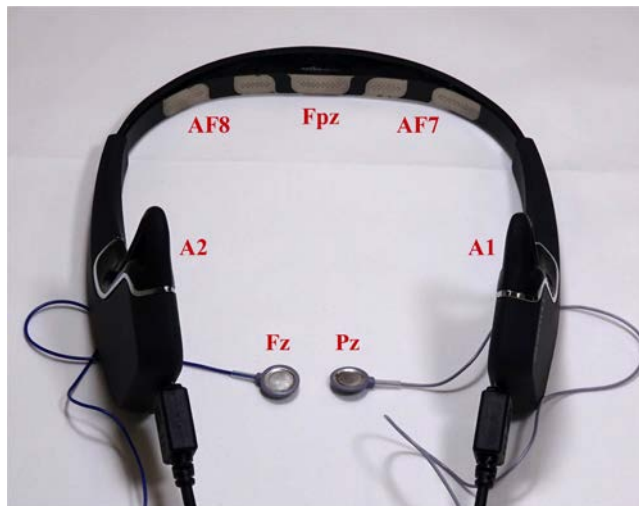


FIGURE 2. Electrode positioning on the “muse” wearable biosignal acquisition device. The *Fpz* site served as recording reference; adjacent to it, active reference electrodes were located (not labeled). The *AF7* and *AF8* sites were used for digitizing horizontal electrooculogram (hEOG) and rapid repeated eye-blinks (modes 2-4). The *A1* and *A2* sites were used for digitizing jaw electromyogram (EMG, mode 2) and vertical EOG (VEOG, mode 3) in combination with *AF7/AF8*, and to detect single eye-blinks. Alpha-band electroencephalogram activity was recorded between the *Pz* and *Fz* sites (mode 4).

We compared four control modes predicated on different combinations of actions, one involving acceleration time-series only and three electrical bio-signals only (Table 1). In all modes, a standby/resume command was provided and the participant was required to disable and re-enable the robot between pawn groups; reflecting the requirement that assistive devices should not enable accidentally during daily activities, highly infrequent and effortful actions needed to be repeated rapidly to enact the command: head tilting (mode 1) or rapid eye blinking (modes 2-4).

As detailed below, the base rotation axis was proportionally controlled directly by the participant when steering the arm towards the intended pawn or cup, based on sideways head

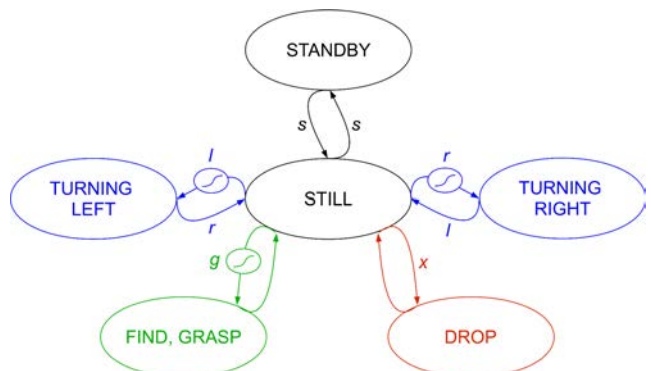


FIGURE 3. Control state machine. The robot transitioned between standby mode (all motion commands ignored) and still state upon detection of an effortful action (*s*), namely either head tilting (mode 1) or repeated eye blinking (modes 2-4). Arm base steering was set according to three discrete states (blue; turning left, still, turning right), transitions between which were driven by brief horizontal movements (*l,r*) of the head (mode 1) or eye-gaze (modes 2-4); entering either rotation state, movement intensity determined arm base rotation rate according to a sigmoid scaling function. Following detection of a grasping command (*g*), namely nodding (mode 1), jaw clenching (mode 2) or eye blinking (modes 3-4), the system transitioned to a state (green) wherein arm steering adjustment and grasping were performed automatically; upon entering this state, nodding sharpness (mode 1), clenching intensity (mode 2), vertical eye-gaze displacement (mode 3) or hand grasping force (mode 4) determined the grasping force applied by the robot according to a sigmoid scaling function. When the arm was steered to face a cup while holding a pawn (*x*), the system transitioned to a state (red) wherein a dropping sequence was performed automatically. The automated control states (red, green) could also be entered from the turning states (transitions not shown).

rotation (mode 1) or horizontal eye movement (modes 2-4). Left and right movements allowed for a transition between three discrete states for base steering control: “still”, “rotating towards left” and “rotating towards right”. In the “still” state, movement initiates rotation in the corresponding direction at a proportionally-controlled rate; in the other two states, movement in the opposite direction of the ongoing rotation leads to transition back to the “still” state (Fig. 3).

The control modes further differed with respect to the commands triggering a grasping action and setting the corresponding force level. In mode 1, grasping was triggered by nodding and the force level was specified by nod steepness (rapidity). In mode 2, grasping was triggered by jaw clenching and the force level was specified by duration and intensity of clenching. In both modes 3 and 4, grasping was triggered by eye blinking and the force level was specified by a separate action performed between blinking and hearing an audible click, issued 2 s afterwards. In mode 3, the action consisted of vertical eye-gaze displacement, the bottom corresponding to a higher force level. In mode 4 the action consisted of performing near-isometric squeezing of a hard cylindrical object with the right hand: to specify light force level, the object was grasped and released with brisk movements and a very light squeeze (<1 kg), whereas to specify strong force level, the squeeze was substantially stronger (>10 kg), being applied and released more gradually.

All commands except resume were ignored during standby mode; moreover, to reduce unwanted actions and provide

TABLE 1. Summary of the four implemented control modes.

Mode	Standby/resume	Arm base steering	Grasping trigger	Force selection
1	Repeated head tilting (accel. <i>XYZ</i>)	Sideways head rotation (accel. <i>XYZ</i>)	Nodding (accel. <i>XYZ</i>)	Nodding steepness (accel. <i>XYZ</i>)
2	Rapid repeated eye-blink (AF7+AF8)	Horizontal eye movement (hEOG, AF7-AF8)	Jaw clench event (EMG, A1+AF7+ AF8+A2)	Jaw clench integral (EMG, A1+AF7+ AF8+A2)
3	Rapid repeated eye-blink (AF7+AF8)	Horizontal eye movement (hEOG, AF7-AF8)	Single eye-blink (A1+A2)	Vertical eye movement (vEOG, A1-AF7- AF8+A2)
4	Rapid repeated eye-blink (AF7+AF8)	Horizontal eye movement (hEOG, AF7-AF8)	Single eye-blink (A1+A2)	Alpha-band activity (EEG, ERD/ERS, Pz-Fz)

Gestures are herein associated to the commands and corresponding signals (recording sites). All electrical signals were referenced to the *Fpz* site. hEOG/vEOG: horizontal/vertical electrooculogram, EMG: electromyogram, EEG: electroencephalogram, ERD/ERS: electroencephalogram event-related desynchronization/synchronization. See text for detailed algorithm descriptions.

windows of unconstrained movement for the participant, each decoded command was followed by a short refractory time during which no further actions were considered. The specific methods used for detecting these actions and processing the underlying signals are detailed in the following subsections. The corresponding algorithms were implemented in MatLab 2012b (MathWorks Inc., Natick MA, USA); their preliminary implementation code is publicly available [47]. The present experiment was run in a dedicated thread and communicated via TCP/IP to the robot control thread.

As the focus here is on feasibility demonstration, we acquired multiple-session data to evaluate controllability consistency in a setting inherently representative of the ceiling-level performance attainable with the interface: each of the 4 control modes was tested 7 times, in arbitrary order, by a healthy subject (participant “A”, 32 year-old, male, 23 years of formal education) who was directly involved in developing the interface and therefore already extensively trained to operate it. Each session required the manipulation of 18 pawns, for a total of 126 actions per mode. We underline that all internal control variables were entirely inaccessible during task performance; hence, detailed knowledge could not have provided any kind of unfair advantage beyond the proficiency attainable in principle by any arbitrary participant after sufficient training. We also confirmed controllability with an additional subject (participant “B”, 30 year-old, female, 20 years of formal education) who was entirely naive to the experiment and without any previous BCI/BMI experience and who practiced for approx. 2 hours prior to performance measurement. All raw time-series and associated logs are publicly available [47]. Written informed consent was provided and all procedures were in accordance with protocols approved by the local institutional review board (approval n. A15072, date: 10.10.2014, principal investigator: Y.K.).

C. ROBOT ARM HARDWARE AND CONTROL

The mechanics were adapted from a commercially-available kit (AL5D; Lynxmotion Inc., Pekin IL, USA), providing a forearm and arm length, respectively, of 23 and 15 cm and

a gripper with a maximum aperture of 2.5 cm (Fig. 1a). The arm axes and gripper were modified and actuated using digital servomotors (Hitec RCD Inc., Chungcheongbuk-do, Korea), models HS-5805MG (shoulder and elbow), HS-6545MG (base rotation and wrist) and HS-5485HB (wrist rotation and gripper). Two color cameras with embedded processing (CMUcam5 “pixy”; Carnegie Mellon University, Pittsburgh PA, USA) were installed 5 cm above the gripper, oriented 30° downward and inward; these open-source hardware devices provided a resolution of 640x400 and real-time color signature-based recognition at a rate of 50 Hz (Fig. 1b) [48]. Two 0.2” force-sensitive resistors (FSR400; Interlink Electronics Inc., Camarillo CA, USA) were mounted on opposite sides in the gripper. Time-of-flight infrared distance sensors (VL6180X; ST Microelectronics, Geneve, Switzerland) and an inertial motion unit (UM7; CH Robotics Inc., Payson UT, USA) were also present but not utilized in this experiment.

The robot arm was connected to a custom-designed control box, for which detailed fabrication materials are freely available from the authors upon request. The system was based on an embedded PC (EBC545; Nexcom Inc., Taipei, Taiwan). The digital servomotors were interfaced through individual serial ports (PCM-3643; Advantech Inc., Taipei, Taiwan) and custom electronics enabling single-wire bidirectional communication using a proprietary protocol and providing galvanic isolation. The force sensors were interfaced through a dedicated analog-to-digital converter (PCM-3718) with a custom front-end amplifier and filter.

The robot arm was controlled by code written in MatLab 2012b and C language for hardware interfacing, running on the embedded PC and publicly available [47]. The code operated as a TCP/IP server and accepted commands from the previously-mentioned thread implementing real-time signal analysis.

As previously indicated, the control system operated in hybrid mode, allowing direct control of a robot axis by the user and also being capable of autonomous, vision-guided execution of high-level commands. After activation (resume command), the participant directly drove the arm base

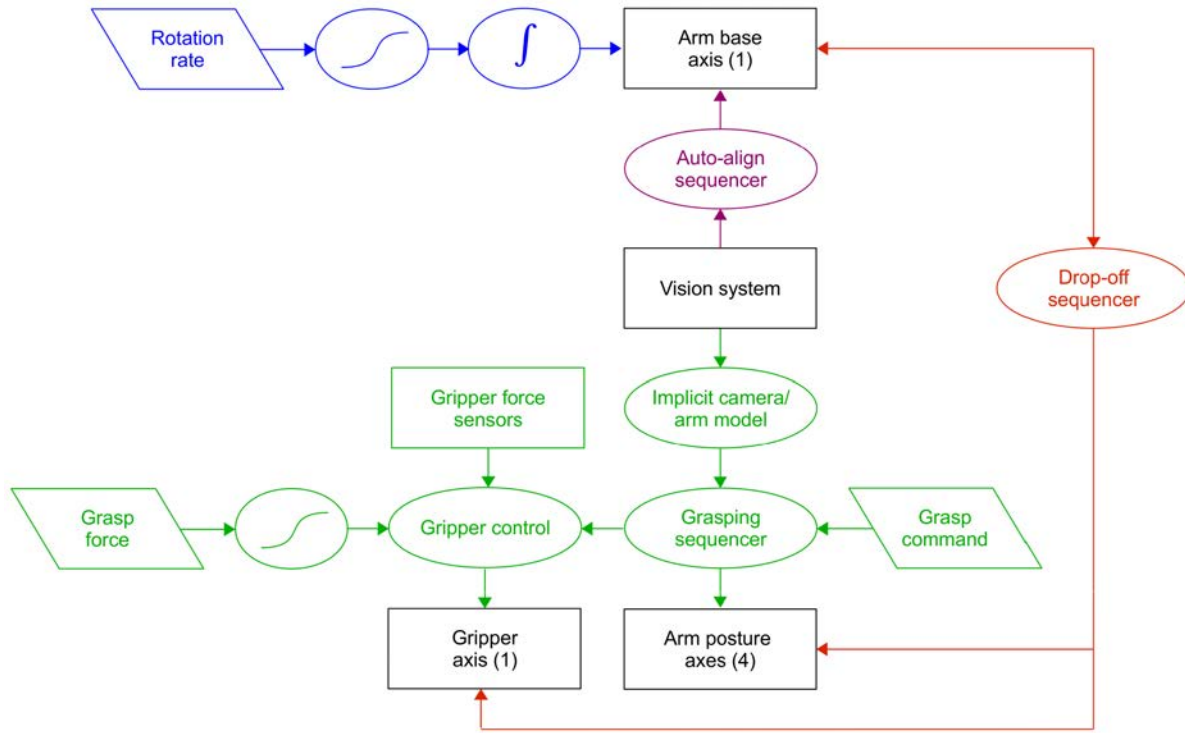


FIGURE 4. Conceptual diagram of the control system. Colors represent sections active at different times during interaction as per Fig. 3. After system activation, the participant directly controlled arm base rotation direction and rate, which was scaled via a sigmoid function and subsequently integrated (blue). Upon detection of the grasping command, control of this axis was transferred to an algorithm performing precise steering towards the nearest pawn under vision guidance (purple). Afterwards, an implicit model of the cameras and arm was used to interpolate a grasping posture, which was selected depending on pawn color; after execution of the corresponding sequence, the gripper was closed up to a force level set by the participant and also weighted by a sigmoid function (green). With the gripper thus holding an object, the participant again directly controlled base rotation, until the arm faced either of the two cups, at which point a dropping sequence was initiated (red).

rotation direction and rate, which was scaled via a sigmoid function of the form $y = (1 + e^{-k(x-x_0)})^{-1}$, where x represents the raw rotation rate setting as measured according to the decoding procedures described below (for sideways head rotation, and horizontal eye movement) and y represents the rotation rate actually executed, which was subsequently integrated to yield the base rotation angle. Sigmoid scaling was motivated to enhance responsiveness in the intermediate range of the rate setting, improving controllability; analogous uses of sigmoid functions in other scenarios have been extensively described [49].

In this experimental task, as in practical applications of assistive robots, precise alignment toward intended targets is challenging. Addressing this issue, upon detection of the grasping command, control of this axis was transferred to an algorithm performing fine alignment towards the nearest pawn under vision guidance (Fig. 3, Fig. 4). An autonomously-executed grasping sequence was thereafter initiated (Fig. 1d). Object detection was performed based on hue, area and size ratio, after which distance and, subsequently, angles for the shoulder, elbow, wrist and wrist rotation axes were estimated via polynomials representing compact, implicit models of the cameras and arm kinematics. In particular, predicated on the fact that

observation was performed from a fixed vantage point (vision system origin) the relationship between object distance and co-ordinates on the camera planes could be represented as follows

$$\begin{cases} x_L(d) = p_{1,1}d^2 + p_{1,2}d + p_{1,3} \\ y_L(d) = p_{2,1}d^2 + p_{2,2}d + p_{2,3} \\ x_R(d) = p_{3,1}d^2 + p_{3,2}d + p_{3,3} \\ y_R(d) = p_{4,1}d^2 + p_{4,2}d + p_{4,3} \end{cases}$$

where x_L , y_L , x_R , y_R represent the co-ordinates of the centre-of-mass on the acquired images in pixels, d the object distance in mm, and $p_{i,j}$ are pre-determined, fixed calibration coefficients. After estimation of d , the target joint angles for object pick-up were determined with

$$\begin{cases} \theta_{\text{shoulder}}(d) = q_{1,1}(d + \delta)^3 + q_{1,2}(d + \delta)^2 \\ \quad + q_{1,3}(d + \delta) + q_{1,4} \\ \theta_{\text{elbow}}(d) = q_{2,1}(d + \delta)^3 + q_{2,2}(d + \delta)^2 \\ \quad + q_{2,3}(d + \delta) + q_{2,4} \\ \theta_{\text{wrist}}(d) = q_{3,1}(d + \delta)^3 + q_{3,2}(d + \delta)^2 \\ \quad + q_{3,3}(d + \delta) + q_{3,4} \\ \theta_{\text{wrist_rotation}}(d) = q_{4,4} \end{cases}$$

where θ represent the joint angles scaled to the servomotor range in $[0, 1]$, d is the object distance in mm estimated as above, δ is a correction constant determining where the object is centered in the gripper, and $q_{i,j}$ are pre-determined calibration coefficients.

The polynomial coefficients $q_{i,j}$ and the correction constant δ were automatically selected between two sets to implement a different posture depending on object features (in this experiment, pawn color; Fig. 1c). After the arm reached the target pawn by means of following an interpolated trajectory to the target position determined as indicated above, the pawn was grasped with the force level set by the participant, also weighted by a sigmoid function. The force-sensitive resistor readings were approximately linearized via a predetermined function and summed, accounting for respective sensitivity; however, because reading accuracy and reproducibility were limited, a steep sigmoid function was chosen to effectively implement binary choice between weak and strong force. Detection of insufficient mechanical resistance always led to complete squeezing when high force was requested (Fig. 1b); moreover, for safety reasons, the control parameters were set so that the steel pieces would not be dropped even when requesting weak force, without affecting the command decoding accuracy measurements described below. When the gripper was holding a pawn, direct control of base steering was relinquished to the user until the arm was directed to either cup, at which point a pre-set dropping sequence was executed.

D. COMMAND RECOGNITION FROM HEAD MOVEMENTS (ACCELEROMETER)

1) REPEATED HEAD TILTING (STANDBY/RESUME)

For ongoing detection of repeated head tilting (mode 1), the acceleration vectors were extracted for the $[-4, 0]$ s window and filtered at 0.25-5 Hz through an order 25 finite impulse-response (FIR) filter. The signals were epoched according to the zero-crossing points of component Z , after which its peak magnitude was located within each epoch, and corresponding times and acceleration vectors were extracted. If at least 3 zero crossings occurred, the epochs were sorted according to the Z component magnitude peaks, and separately for each component, the difference was calculated between the average of the two top and bottom ones. For this command to be detected, the difference needed to be larger for the Z than the XY components and between 600-2400 mg, with the corresponding time interval being between 1.5-2.5 s. After detection, further commands were inhibited for 4.5 s. In practice, issuing this command required quickly swinging the head sideways by approximately 30 degrees.

2) SIDEWAYS HEAD ROTATION (ARM BASE STEERING)

For ongoing detection of sideways head rotation (mode 1), the acceleration vectors were extracted for the $[-2, 0]$ s window. The average standard deviation of their components

in the $[-1.6, -0.8]$ s window was calculated. If it exceeded 30 mg, the analysis did not proceed further (spurious activity). Otherwise, the X and Z signals were averaged and the difference between sample pairs separated by 200 ms was calculated via a filter having coefficients $[1, 0, \dots, 0, -1]$ and smoothed using a 100 ms-span moving average filter; an analogous set of operations was performed for the Y signal separately. The maximum and minimum in the $[-0.8, 0]$ s window were found for the XZ signal, and the corresponding amplitude difference was calculated for this signal and for the Y signal. A head rotation event occurred if the difference for the XZ signal exceeded 30 mg and that of the Y signal; however, the corresponding command was not issued until after 330 ms to allow detection of a potentially stronger movement within this time interval. The base rotation rate was determined by the XZ signal maximum-minimum difference, rescaled according to a sigmoid function having $x_0 = 150$ mg and $k = 0.07 \text{ mg}^{-1}$, and its direction was inferred from the magnitude of the maximum and minimum. After detection, further commands were inhibited for 1.2 s. Moreover, to reduce the probability of misrecognition of nodding as sideways head rotation, the rotation command was not issued if the maximum of the X signal in the $[-1, 0]$ s window minus the mean of the same signal in the $[-2, -1]$ s window plus twice the difference between the mean Y signal in $[-2, -1]$ s and the minimum of the same in $[-1, 0]$ exceeded 250 mg. In practice, this command allowed for steering the robot arm base with small, brisk head movements that did not interfere with maintaining uninterrupted sight of the robot.

3) NODDING (GRASPING TRIGGER AND FORCE SETTING)

For ongoing detection of nodding (mode 1), the acceleration vectors were extracted for the $[-6, 0]$ s window and filtered at 0.25-5 Hz through an order 25 FIR filter. The maximum and minimum of the X component in the $[-4, 0]$ s window were determined. Nodding was detected if the corresponding difference was between 300-1800 mg and all the following conditions were met: the standard deviation of the same component in the same time window was between 15-300 when divided by the average standard deviation of the three components in the $[-5, -4]$ s window, between 1-5 when divided by the standard deviation of the Y component in the $[-4, 0]$ s window and between 3-20 when divided by the standard deviation of the Z component in the $[-4, 0]$ s window. Nodding intensity was determined based on the peak-to-peak amplitude of the X component during $[-4, 0]$ s, then rescaled according to a sigmoid function having $x_0 = 1250$ mg and $k = 0.1 \text{ mg}^{-1}$. The corresponding command was not issued until after 500 ms to allow detection of a potentially stronger movement within this time interval. After detection, further commands were inhibited for 5 s. In practice, a brief period of head immobility in straight posture was required, followed by a sharp nod, the amplitude and speed of which together determined the measured strength.

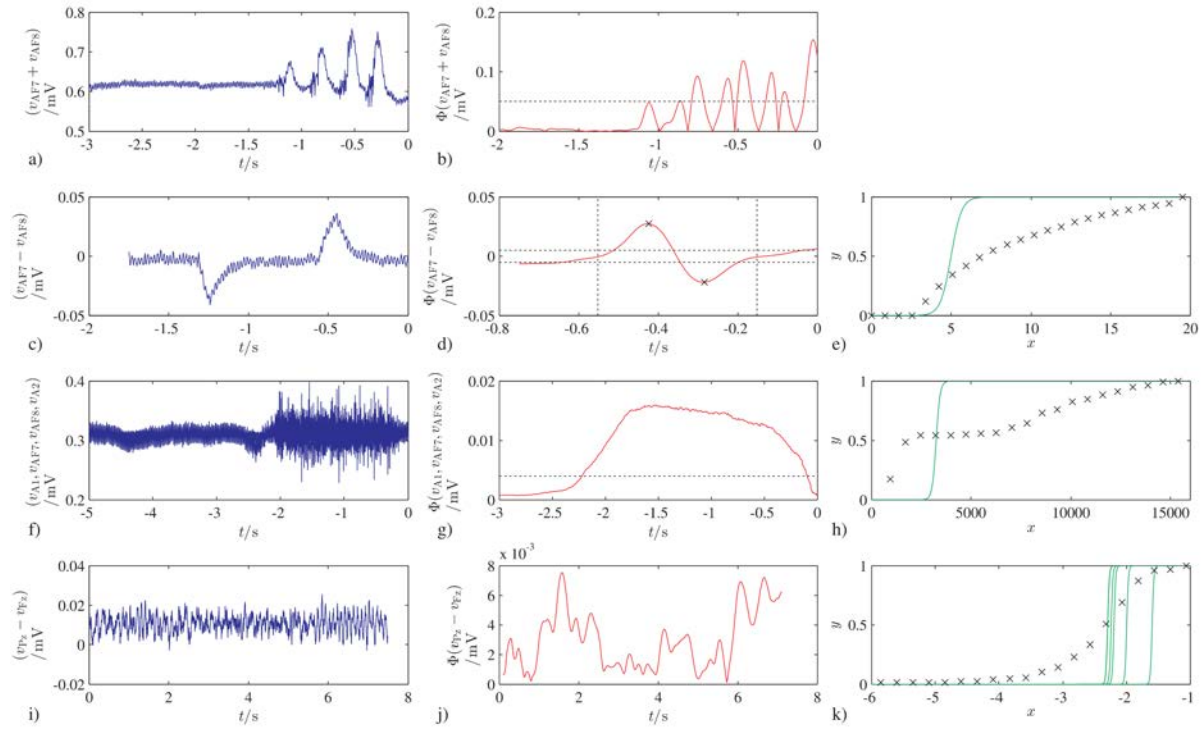


FIGURE 5. Raw (blue) and processed (red) bio-signals from representative trials, and corresponding scaling functions. See text for description of the associated algorithms. a) Raw and b) processed signals from rapid repeated eye-blink; dashed line denotes detection threshold. c) Raw and d) processed signals from horizontal eye movements (hEOG); dashed lines denote detection thresholds and time-window for identification of minimum and maximum (black crosses). e) Scaling function yielding base rotation rate (y) given horizontal eye movement amplitude (x , green), and associated cumulative distribution of issued commands (y , black crosses). f) Raw and g) processed signals from jaw clenching; dashed line denotes detection threshold. h) Scaling function yielding grasping force (y) given jaw clench intensity (x , green), and associated cumulative distribution of issued commands (y , black crosses). i) Raw and j) alpha-band processed fronto-parietal electroencephalogram (EEG), see also Fig. 6. k) Scaling functions (differing parameters between sessions) yielding grasping force (y) given alpha-band activity intensity (x , green), and associated cumulative distribution of measured values (y , black crosses).

E. COMMAND RECOGNITION FROM ELECTRICAL BIO-SIGNALS

1) RAPID REPEATED EYE-BLINK (STANDBY/RESUME)

For ongoing detection of rapid repeated eye-blink (modes 2-4), signals from the AF7 and AF8 sites (Fig. 5a) were extracted for the $[-3, 0]$ s window, summed, demeaned and filtered at 2-5 Hz through an order 50 FIR filter. The difference between sample pairs separated by 200 ms was calculated via a filter having coefficients $[1, 0, \dots, 0, -1]$; the resulting signal was rectified and cropped to the $[-2, 0]$ s window (Fig. 5b). The number of crossings with respect to a first threshold set to $50 \mu\text{V}$ and the signal average during the supra-threshold intervals were calculated. If these exceeded, respectively, 6 and $75 \mu\text{V}$, a rapid repeated eye-blink was deemed to have occurred and a corresponding command transitioning the system between the stand-by and active states was issued. After detection, further commands were inhibited for 3 s. This command was extracted from the sum of the potentials at the AF7 and AF8 sites, instead of the sites indicated below for single blinks and vertical EOG, to minimize the risk of spuriously recognizing it during task-unrelated activity (e.g., swallowing and speaking), which lead

to considerably larger fluctuations at the A1 and A2 sites. Furthermore, the optimal thresholds depended on headband positioning and tightness; the thresholds were lowered to $15 \mu\text{V}$ and $25 \mu\text{V}$ throughout the course of the experimental sessions, and the post-detection inhibition interval was elevated to 5 s. In practice, issuing this command required blinking in a pattern unlikely to occur unintentionally for both rapidity and intensity.

2) HORIZONTAL EYE MOVEMENT (ARM BASE STEERING)

For ongoing detection of horizontal eye movements (hEOG; modes 2-4), the difference signal between the AF7 and AF8 sites was calculated for the $[-1.75, 0]$ s window (Fig. 5c), demeaned and filtered at 2-10 Hz through an order 50 FIR filter, then smoothed using a 100 ms-span moving average filter. The difference between sample pairs separated by 20 ms was then calculated via a filter having coefficients $[1, 0, \dots, 0, -1]$, cropped to the $[-0.75, 0]$ s window and detrended. Maxima and minima were determined: if both exceeded $\pm 5 \mu\text{V}$ (Fig. 5d), the detrended average of the signal before the above difference calculation was determined over a window ± 200 ms centered around the maximum of

its modulus. If the modulus of this average exceeded $3 \mu\text{V}$, a horizontal eye movement was deemed to have occurred in the direction given by the sign; however, the corresponding command was not issued until after 250 ms to allow detection of a potentially larger movement within this time interval. The base rotation rate was determined based on the average amplitude specified above, rescaled according to a sigmoid function having $x_0 = 5 \mu\text{V}$ and $k = 3 \mu\text{V}^{-1}$ (Fig. 5e). After detection, further commands were inhibited for 1 s. In practice, this command allowed for steering the robot arm base with small, brisk eye movements that did not interfere with maintaining uninterrupted sight of the robot.

3) JAW CLENCHING (GRASPING TRIGGER AND FORCE SETTING)

For ongoing detection and measurement of the intensity of jaw clenching (EMG; mode 2), signals from the A1, AF7, AF8 and A2 sites (Fig. 5f) were extracted for the $[-5, 0]$ s window, demeaned and filtered at 75-250 Hz through an order 25 FIR filter. The amplitude envelopes were separately calculated from the analytic signal via Hilbert's transform, smoothed using a 500 ms-span moving average filter, cropped to the $[-3, 0]$ s window and averaged across these 4 sites. The resulting signal was then thresholded at $4 \mu\text{V}$ (Fig. 5g). Clenching was detected if the signal rose above and subsequently fell below this threshold during a time interval at least 250 ms long; clenching intensity was measured as the discrete-time integral calculated during the supra-threshold interval, then rescaled according to a sigmoid function having $x_0 = 3250 \mu\text{V}$ and $k = 0.01 \mu\text{V}^{-1}$ (Fig. 5h). After detection, further commands were inhibited for 3 s. In situations of poor signal stability, the processed signal mean during the $[-5, -3]$ s window may be subtracted as the baseline, but this was not done for the present experiment; moreover, when deemed computationally too onerous, computation of the analytic signal may be replaced by simpler, sliding window-based amplitude measures.

4) SINGLE EYE-BLINK (GRASPING TRIGGER)

For ongoing detection of single eye-blink events (modes 3-4), signals from the A1 and A2 sites were extracted for the $[-2.4, 0]$ s window, summed and demeaned, and the difference between sample pairs separated by 200 ms was calculated via a filter having coefficients $[1, 0, \dots, 0, -1]$. The resulting signal was filtered using a 100 ms sliding window, rectified and cropped to the $[-2, 0]$ s window. The sub-segments having a negative first time-derivative and amplitude greater than $70 \mu\text{V}$ were subsequently extracted, and a single eye-blink was deemed to have occurred if at least one such segment was identified and the peak amplitude during it was greater than $75 \mu\text{V}$. To increase timing accuracy, the occurrence time of the eye-blink was refined a-posteriori, setting it to the mid-point between minimum and maximum of the smoothed (100 ms) difference signal measured between the A1/A2 and AF7/AF8 sites. Single eye-blink detection was performed primarily based on the A1/A2 sites, as the signal

at these sites appeared less susceptible to spurious detection due to eyebrow movements; it was resorted to in modes 3-4 because reliable triggering could not be attained based on the same signals considered for force level setting (described in the next sub-sections).

5) VERTICAL EYE-GAZE DISPLACEMENT (GRASPING FORCE SETTING)

For measuring vertical eye-gaze displacement (vEOG; mode 3) following a single eye-blink event, the difference signal between the average voltages at the A1/A2 and AF7/AF8 sites was considered. Assuming $t = 0$ s as the blink occurrence time, the average voltage in the $[-2, -0.5]$ s window was calculated and subtracted from that of the $[1, 4]$ s window; these time-windows are not critical and may likely be optimized for faster response. The voltage thus measured was then rescaled according to a sigmoid function having $x_0 = 0 \mu\text{V}$ and $k = 50 \mu\text{V}^{-1}$.

6) ALPHA-BAND BRAIN ACTIVITY (GRASPING FORCE SETTING)

For measuring alpha-band brain activity (ERD/ERS; mode 4) following a single eye-blink event, the difference signal between the Pz and Fz sites was considered. Assuming $t = 0$ s as the blink occurrence time, it was epoched between $[0, 7.5]$ s (Fig. 5i) and filtered at 8-12 Hz through an order 250 FIR filter. The amplitude envelope was thereafter calculated from the analytic signal obtained using Hilbert's transform and cropped to the $[0.1, 7.1]$ s window (Fig. 5j), within which average amplitude was calculated for the $[1, 2.5]$ s and $[3.5, 7]$ s sub-windows, which were chosen in preliminary experiments. The resulting values were summed by applying factors f and $(1-f)$ respectively, where f varied between sessions and was 0.72 ± 0.21 (mean \pm standard deviation); their negative sum was rescaled according to a sigmoid function having $x_0 = -2.13 \pm 0.26 \mu\text{V}$ and $k = 75 \mu\text{V}^{-1}$ (Fig. 5k). The negative sign implemented weak force for stronger alpha-band activity. To maximize accuracy, it was chosen to determine the values of x_0 and f empirically based on trials performed immediately prior to each session.

III. RESULTS

Task performance accuracy was quantified as the fraction of trials wherein the target pawn was picked up with the correct force level (for this purpose, binarized as ≥ 0.5 for steel, < 0.5 for felt), then dropped in the correct cup. For brevity, failures due to occasional malfunctions of the robot vision system are not described.

As detailed in Table 2, for participant "A" (ceiling-level), average accuracy across sessions was near-perfect, being approximately 95%, for modes 1-3 but substantially lower, namely, 73%, for mode 4. The variability (standard deviation), approximately 5%, was similar across modes. The average time taken to complete an action (locate, pick-up then drop a pawn) was approximately 43 s for modes 1-3 but 58 s for mode 4; longer time in the latter mode

TABLE 2. Performance summary for participant “A”.

Mode	Signals	Accuracy	Failures	Total commands	Time/action
1	Accelerometer (<i>XYZ</i>)	96±6%	0 (1)	158±21	41±2 s
2	hEOG + EMG	97±6%	2 (3)	216±27	42±3 s
3	hEOG + vEOG + blink	93±5%	0 (1)	216±25	45±2 s
4	hEOG + ERD/ERS + blink	73±5%	0 (2)	253±53	58±4 s

Overall accuracy (percentage of pawns grasped with correct force, dropped in correct cup), failures (times grasping sequence not completed), total number of commands issued, and average time per action (comprising pawn selection, grasping and dropping). Continuous values are reported as mean±standard deviation, failures as median (maximum). hEOG/vEOG: horizontal/vertical electrooculogram, EMG: electromyogram, ERD/ERS: electroencephalogram event-related desynchronization/synchronization.

was due to the participant seeking greater concentration prior to issuing the grasping command. Out of these times, on average, 15.8 ± 4.0 s and 5.5 ± 0.2 s were required by the robot arm to execute, under autonomous control, pawn grasping and dropping, respectively. The total number of commands issued was, on average, 158 in mode 1, 216 in modes 2 and 3, and 253 in mode 4; the smaller value for mode 1 appeared to reflect superior proportional control of the base rotation rate, whereas the large value for mode 4 compared to 2 and 3 was plausibly due to generally lower participant confidence in this mode. For participant “B” (naive), the accuracy was equally 89% in modes 1 and 2; the average times/action were, respectively, 63 and 89 s, with the corresponding total number of commands being 161 and 355; for this participant, modes 3 and 4 had to be aborted due to inability to control eye blinking, leading to a prohibitively high number of undesired grasping actions.

Consideration of the cumulative distributions of base rotation rate in mode 1 (data not shown) and modes 2-3 (Fig. 5e) and of grasping force in mode 2 (Fig. 5h), mode 3 (data not shown) and mode 4 (Fig. 5k) confirmed that based on the methods specified above, it was possible not only to decode discrete commands with high accuracy but also to specify continuous parameters associated with them. For the case of base steering, the majority of commands had associated intensity close to the steepest region of the sigmoidal transfer function, representing the fact that participant “A” had become experienced with the system response and could exploit it to obtain the desired compromise between steering speed and positioning accuracy. Contrariwise, for grasping force, particularly in mode 2, awareness that the transfer function effectively embodied a threshold led to preferential choice of either very high or very low settings.

The average alpha-band responses recorded in mode 4 are shown in Fig. 6. Performing light squeezing to select low force was associated with a clearly biphasic ERD/ERS pattern: squeeze application lead to initial desynchronization peaking at ≈ 0.7 s, followed by synchronization peaking at ≈ 2.3 s, and squeeze release in response to the audible click (issued at 2 s) led to a further desynchronization peaking at ≈ 3.4 s, followed by a larger, more persistent synchronization having a plateau between ≈ 6.5 - 8.2 s. By contrast, application of a strong squeeze led to a mono-phasic ERD/ERS

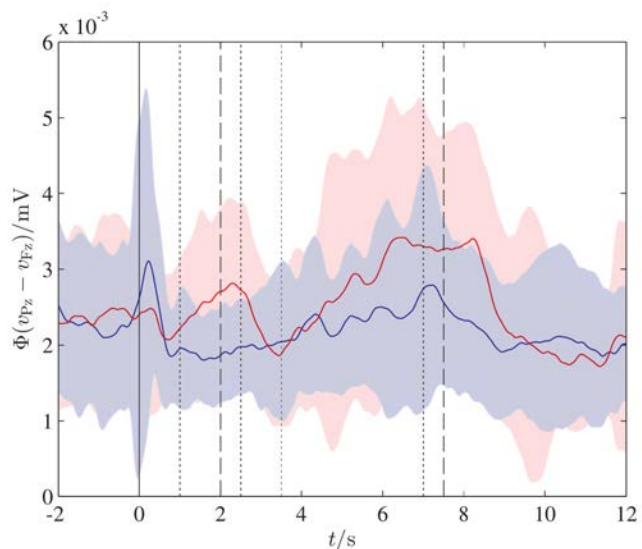


FIGURE 6. Event-related desynchronization/synchronization (ERD/ERS) effect measured for alpha-band activity of the electroencephalogram recorded between the *Pz* and *Fz* sites. Solid lines denote average over all pooled high- and low-force trials (blue and red, respectively), and shaded areas indicate 1 standard deviation. Dashed lines at 2 s and 7.5 s mark, respectively, approximate onsets of audible click (prompting release) and robot movement initiation; dotted lines denote averaging windows (see text). A biphasic pattern was well evident for low-force trials (red), whereas the average response was mono-phasic and post-movement synchronization was weaker for high-force trials (blue). See text for description of corresponding actions. Smoothing with 500 ms span applied for visualization.

pattern, wherein the first (de)synchronization wave was abolished; instead, desynchronization peaked at ≈ 1.6 s, followed by shallower synchronization peaking at ≈ 7.2 s. A-posteriori re-analysis of the data revealed that an accuracy of 81% might theoretically have been attainable by setting the averaging windows to [1, 2.5] s and [6.5, 8.5] s, with $f = 0.68$ and $x_0 = -2.39 \mu\text{V}$; however, substantial inter-session variability remained evident.

IV. DISCUSSION

Previous research in this area has demonstrated computer and robot control leveraging upon diverse bio-signal sets including EEG only, EOG only, combined EEG and EOG, and EMG. Only a fraction of the existing studies

have been conducted with consumer-grade wearable devices rather than research-grade high channel-count systems, and there is considerable heterogeneity in the control approach, with some reports focusing on proportional and others on state-based (discrete, sparse) techniques and few integrating the two [7]–[9], [11], [12], [25]–[27], [37], [50]–[52]. In the present proof-of-concept study, we demonstrated a system-level concept, drawing upon current trends in assistive robotics, biosignal-based human-machine interfaces and wearable technology, and proposed a hybrid control approach intended for eventually controlling wheelchair-mounted robotic manipulators and meal-assisting robots; here, the focus was on demonstrating in-principle practical usability of a representative low-cost wearable interface for robotic arm control.

The control approach that we advocate is hybrid at two levels. We deem this approach as an effective compromise between robot controllability and maintaining the user goal-focused rather than process-focused. First, robot arm steering combines a discrete and a proportional component: it is controlled by a state machine driven by discrete commands, but the rotation rate is proportionally set by the user via the sharpness of head or eye movement. Second, after the robot has been steered to the approximate target direction, a sparse approach is followed, wherein the user only needs to issue a single command, after which fine steering and grasping with an object-dependent posture are completed automatically; however, also for the grasping command, the intensity of the corresponding action (nodding, clenching, vertical eye movement or hand grasping) proportionally controls the force level applied by the robot. Consideration of hybrid control for practical interfaces has been advocated in several recent studies [39], [42], [46], [52].

While high-precision eye-gaze direction reconstruction using EOG and optical tracking has been previously demonstrated, here, rather than steering robot direction directly, we opted for differential control, allowing the user to set the direction and rate of arm base rotation instead. This is because in preliminary experiments, we had determined that this differential approach is less demanding on EOG signal quality and therefore better suited for use with a consumer wearable device, which imposes EOG recoding from sub-optimal electrode locations. We also avoided providing feedback via a graphical user interface to maintain the user goal-focused because the small eye or head movements required for differential control integrate to zero over small time-scales, thus allowing maintenance of uninterrupted sight of the robot and target [8], [25], [53]. Our results underline that successful proportional control based on EOG, eye blinking, jaw EMG and EEG is, in principle, feasible even given the considerable electrode location and signal quality constraints associated with a consumer-grade headband marketed for a different purpose, namely, as a relaxation aid; moreover, the ongoing analysis algorithms we described are relatively undemanding and thus suitable for porting on embedded microcontrollers.

We provide preliminary data on ceiling-level performance attainable with 4 control modes by implementing the above-described hybrid approach based on different bio-signal combinations. Overall, modes 1–3 yielded comparable and reproducible performance, while mode 1, based on accelerometer signals, required a smaller number of commands to complete the task, suggesting better proportional control of robot base rotation with respect to horizontal EOG, even though the time needed to complete the task was similar (Tables 1 and 2). This control mode, however, requires effortful head movements to issue the grasping and standby/resume commands, which may be problematic for some patients; depending on the specific situation, one could opt for mode 1, mode 2 or a combination of them, e.g., driving base rotation with accelerometer signals and choosing jaw clenching and repeated eye blinking for controlling grasping and standby/resume. For these two modes, the naive participant also attained a high degree of accuracy, even though the time required for task completion was predictably longer. For the experienced participant, control mode 3, based exclusively on EOG and eye blinking, also provided similar performance; however, the naive participant was unable to use this mode due to excessive eye-blinking, underlining that even though it was the most parsimonious one in terms of neurological integrity requirements, it is unlikely to be the most viable one. Because the ongoing analysis algorithms were computationally undemanding, response latency was determined primarily by the additional lag imposed after decoding each command to allow for confirming its intensity: for the case of base steering, this was ≈ 330 and ≈ 250 ms for control modes 1 and 2–4, respectively. Overall, the task performance accuracy attained in modes 1–2 was high and reproducible across sessions and for both the experienced and naive participant, and the accuracy level was in line with representative studies in this area, some of which had involved considerably more complex acquisition setups [7], [9]–[11], [16], [27], [34], [50], [54]. Plausibly owing to leveraging on multiple bio-signals and the tailored detection algorithms that were developed, our evaluation thus yielded a more positive outlook compared to a recent analysis of two other consumer-grade EEG devices [55]. It is important to underline that here, independent annotation of all individual actions was not performed; thus, accuracy for the task as a whole was the only performance metric considered and recognition accuracy at the single-command level was not measured.

In mode 4, task duration was elongated and grasping force decoding was substantially less accurate, being 73%. This figure overlaps the variability, namely, 60–80%, observed across previous studies on gesture or force level recognition using ERD/ERS [56]–[58]. More generally, higher accuracy, in line with modes 1–3, has been previously attained with purely EEG-based control, particularly with recourse to P300-based paradigms: here, such approach was deemed unsuitable due to event synchronization difficulty on a consumer wearable platform streaming continuous data and due to additional user interface elements requirements; furthermore, we were

constrained with respect to the number of electrodes and data acquisition hardware [16], [46], [59]. Higher hand grasping force recognition accuracy has been previously attained based on ERD/ERS computed from high-density EEG, underlining the importance of topographical information, which was inaccessible here; moreover, the relationship of ERD/ERS with grasping force and duration remains incompletely understood, with evidence that it more closely indexes motor planning than downstream execution [59]–[62]. In the present experiment, a two-phase grasping paradigm was adopted, with initiation marked by an eye blink and release triggered by an audible click 2 s afterwards. It was developed to maximize the ERD/ERS difference between weak and strong grasping conditions and yielded the highest accuracy we could obtain using the wearable device under consideration. For weak grasping, a biphasic ERD/ERS response was observed, the first half of which was abolished for strong grasping; the amplitude of the second ERS was larger for weak rather than strong grasping: such pattern is suggestive of more protracted cortical activation when maintaining strong grasping (Fig. 6). To the authors' knowledge, this paradigm is novel and worthy in itself of general consideration in ERD/ERS-based force level estimation. Because the participant had extensive practice, the observed difference plausibly included volitional control elements; in this regard, we note that higher control accuracies have been reported based on volitional modulation of occipital alpha rhythm, and while here we focused on central alpha activity because the aim was direct grasping force decoding, alternative EEG electrodes positioning should be considered [16], [63], [64].

We aimed at delivering a compromise between ease of control and flexibility for assistive applications: according to the proposed hybrid approach, the user retains unconstrained control in steering the robot toward the target object, and engaging autonomous guidance afterwards relieves the user from the burden of fine adjustment of the joints to attain intended postures, maintaining the goal focus. We demonstrated this approach using a desktop robotic arm whose 5 + 1 degree-of-freedom kinematics are analogous to existing assistive robotic manipulators, aiding clinical translation of the results [3], [5], [7], [38], [50], [65]. This experiment relied on elementary object detection via hue and geometric features, but the approach is viable with arbitrary vision systems, e.g., capable of recognizing objects belonging to specific classes through deep learning techniques; furthermore, it is, in principle, applicable to both image-based and position-based vision servoing [5], [44], [46], [66]–[68]. Existing literature on assistive arms poses limited emphasis on control of force and posture, two elements important for practical usability. Here, we sought a means of controlling them without overwhelming the user and demonstrated it via colored pawns requiring a certain pick-up posture (straight vs. sideways) and grasping force (steel vs. felt). We propose that arm posture is automatically chosen from a repertoire based on visual features because in practical applications, a finite number of object categories are encountered and each requires a

specific posture, e.g., operating a door handle vs. retrieving a plastic bottle for a wheelchair-mounted arm, or picking up rice vs. meat for a meal-assistance robot. Contrariwise, we propose that grasping force, or where appropriate, joint torque, is proportionally set by the user without discretization constraints, as the level required is highly situation-dependent and may be subjective, e.g., the user may have pre-existing knowledge regarding the force required to operate a door handle or to spear a certain food item using a fork [36], [69]–[71]. Future research on the present problem should also be conducted adopting a more control theory-centric approach, aiming to optimize system performance and enhance robustness for example by devising practical control laws for tracking, and by explicitly taking into account actuator dynamics and parameter uncertainties [72]–[74].

We demonstrated the possibility of successful control of a 5 + 1 degrees-of-freedom robot arm based on a consumer wireless headband combined with tailored detection algorithms and a hybrid control approach, which were described in precise detail. Future research will focus on extending this preliminary work to adaptive choice of detection parameters, evaluating the control accuracy in larger and representative cohorts of healthy participants, integrating the system with pre-existing wheelchair-mounted and meal-assistance robots, and assessing its ecological performance for a representative population of patients with diverse neurological diseases performing routine tasks.

REFERENCES

- [1] M. Pazzaglia and M. Molinari, "The embodiment of assistive devices—From wheelchair to exoskeleton," *Phys. Life Rev.*, vol. 16, pp. 163–175, Mar. 2016.
- [2] S. Allin, E. Eckel, H. Markham, and B. R. Brewer, "Recent trends in the development and evaluation of assistive robotic manipulation devices," *Phys. Med. Rehabil. Clin. North Amer.*, vol. 21, no. 1, pp. 59–77, Feb. 2010.
- [3] V. Maheu, J. Frappier, P. S. Archambault, and F. Routhier, "Evaluation of the JACO robotic arm: Clinico-economic study for powered wheelchair users with upper-extremity disabilities," in *Proc. IEEE Int. Conf. Rehabil. Robot.*, Zürich, Switzerland, Jul. 2011, pp. 1–5.
- [4] H. Wang *et al.*, "The personal mobility and manipulation appliance (PerMMA): A robotic wheelchair with advanced mobility and manipulation," in *Proc. IEEE Eng. Med. Biol. Soc. Annu. Int. Conf.*, San Diego, CA, USA, Sep. 2012, pp. 3324–3327.
- [5] H. Jiang, J. P. Wachs, and B. S. Duerstock, "Integrated vision-based robotic arm interface for operators with upper limb mobility impairments," in *Proc. IEEE Int. Conf. Rehabil. Robot. (ICORR)*, Seattle, WA, USA, Jun. 2013, pp. 1–6.
- [6] N. Kawarazaki, D. Stefanov, and A. I. B. Diaz, "Toward gesture controlled wheelchair: A proof of concept study," in *Proc. IEEE Int. Conf. Rehabil. Robot. (ICORR)*, Seattle, WA, USA, Jun. 2013, pp. 1–6.
- [7] M. Ison, I. Vujaklija, B. Whitsell, D. Farina, and P. Arتمiadis, "High-density electromyography and motor skill learning for robust long-term control of a 7-DoF robot arm," *IEEE Trans. Neural Syst. Rehabil. Eng.*, vol. 24, no. 4, pp. 424–433, Apr. 2016.
- [8] M. I. Rusydi, M. Sasaki, and S. Ito, "Affine transform to reform pixel coordinates of EOG signals for controlling robot manipulators using eye motions," *Sensors*, vol. 14, no. 6, pp. 10107–10123, Jun. 2014.
- [9] I. M. Rezazadeh, S. M. Firoozabadi, H. Hu, and S. M. H. Golpayegani, "A novel human-machine interface based on recognition of multi-channel facial bioelectric signals," *Australasian Phys. Eng. Sci. Med.*, vol. 34, no. 4, pp. 497–513, Dec. 2011.

- [10] Y. Hasegawa and S. Oura, "Exoskeletal meal assistance system (EMAS II) for progressive muscle dystrophy patient," in *Proc. IEEE Int. Conf. Rehabil. Robot.*, Zürich, Switzerland, Jul. 2011, pp. 1–6.
- [11] M. Hamedi *et al.*, "Human facial neural activities and gesture recognition for machine-interfacing applications," *Int. J. Nanomed.*, vol. 6, pp. 3461–3472, Dec. 2011.
- [12] P. K. Artempiadis and K. J. Kyriakopoulos, "A switching regime model for the EMG-based control of a robot arm," *IEEE Trans. Syst., Man, Cybern. B, Cybern.*, vol. 41, no. 1, pp. 53–63, Feb. 2011.
- [13] D. Lesenfants *et al.*, "An independent SSVEP-based brain-computer interface in locked-in syndrome," *J. Neural Eng.*, vol. 11, no. 3, p. 035002, Jun. 2014.
- [14] M. Akcakaya *et al.*, "Noninvasive brain–computer interfaces for augmentative and alternative communication," *IEEE Rev. Biomed. Eng.*, vol. 7, pp. 31–49, 2014.
- [15] P. Brunner, L. Bianchi, C. Guger, F. Cincotti, and G. Schalk, "Current trends in hardware and software for brain-computer interfaces (BCIs)," *J. Neural Eng.*, vol. 8, no. 2, p. 025001, Mar. 2011.
- [16] A. Ferreira, W. C. Celeste, F. A. Cheein, T. F. Bastos-Filho, M. Sarcinelli-Filho, and R. Carelli, "Human-machine interfaces based on EMG and EEG applied to robotic systems," *J. Neuroeng. Rehabil.*, vol. 5, p. 10, Mar. 2008.
- [17] G. Townsend and V. Platsko, "Pushing the P300-based brain–computer interface beyond 100 bpm: Extending performance guided constraints into the temporal domain," *J. Neural. Eng.*, vol. 13, no. 2, p. 026024, Apr. 2016.
- [18] J. C. Powers, K. Bieliaieva, S. Wu, and C. S. Nam, "The human factors and ergonomics of P300-based brain-computer interfaces," *Brain Sci.*, vol. 5, no. 3, pp. 318–356, Aug. 2015.
- [19] M. Bamdad, H. Zarshenas, and M. A. Auai, "Application of BCI systems in neurorehabilitation: A scoping review," *Disabil. Rehabil., Assist. Technol.*, vol. 10, no. 5, pp. 355–364, 2015.
- [20] N. Yoshiimura, C. S. Dasalla, T. Hanakawa, M. A. Sato, and Y. Koike, "Reconstruction of flexor and extensor muscle activities from electroencephalography cortical currents," *Neuroimage*, vol. 59, no. 2, pp. 1324–1337, Jan. 2012.
- [21] J. J. Shih, D. J. Krusinski, and J. R. Wolpaw, "Brain-computer interfaces in medicine," *Mayo Clin. Process.*, vol. 87, no. 3, pp. 268–279, Mar. 2012.
- [22] M. D. Murphy, D. J. Guggenmos, D. T. Bundy, and R. J. Nudo, "Current challenges facing the translation of brain computer interfaces from preclinical trials to use in human patients," *Front Cell Neurosci.*, vol. 9, p. 497, Jan. 2016.
- [23] M. Fatoorechi, J. Parkinson, R. J. Prance, H. Prance, A. K. Seth, and D. J. Schwartzman, "A comparative study of electrical potential sensors and Ag/AgCl electrodes for characterising spontaneous and event related electroencephalogram signals," *J. Neurosci. Methods*, vol. 251, pp. 7–16, Aug. 2015.
- [24] M. A. Lopez-Gordo, D. Sanchez-Morillo, and F. P. Valle, "Dry EEG electrodes," *Sensors*, vol. 14, no. 7, pp. 12847–12870, 2014.
- [25] J. Ma, Y. Zhang, A. Cichocki, and F. Matsuno, "A novel EOG/EEG hybrid human-machine interface adopting eye movements and ERPs: Application to robot control," *IEEE Trans. Biomed. Eng.*, vol. 62, no. 3, pp. 876–889, Mar. 2015.
- [26] M. Witkowski, M. Cortese, M. Cempini, J. Mellinger, N. Vitiello, and S. R. Soekadar, "Enhancing brain-machine interface (BMI) control of a hand exoskeleton using electrooculography (EOG)," *J. Neuroeng. Rehabil.*, vol. 11, p. 165, Dec. 2014.
- [27] H. Wang, Y. Li, J. Long, T. Yu, and Z. Gu, "An asynchronous wheelchair control by hybrid EEG–EOG brain–computer interface," *Cognit. Neurodyn.*, vol. 8, no. 5, pp. 399–409, Oct. 2014.
- [28] B. S. Lin, J. S. Pan, T. Y. Chu, and B. S. Lin, "Development of a wearable motor-imagery-based brain-computer interface," *J. Med. Syst.*, vol. 40, no. 3, p. 71, Mar. 2016.
- [29] Y. H. Yu *et al.*, "An inflatable and wearable wireless system for making 32-channel electroencephalogram measurements," *IEEE Trans. Neural Syst. Rehabil. Eng.*, vol. 24, no. 7, pp. 806–813, Jul. 2016.
- [30] N. Kim, T. Lim, K. Song, S. Yang, and J. Lee, "Stretchable multichannel electromyography sensor array covering large area for controlling home electronics with distinguishable signals from multiple muscles," *Appl. Mater. Interfaces*, vol. 8, no. 32, pp. 20176–21070, Aug. 2016.
- [31] J. Wu, L. Sun, and R. Jafari, "A wearable system for recognizing American sign language in real-time using IMU and surface EMG sensors," *IEEE J. Biomed. Health Inform.*, vol. 20, no. 5, pp. 1281–1290, Sep. 2016.
- [32] S. Benatti *et al.*, "A versatile embedded platform for EMG acquisition and gesture recognition," *IEEE Trans. Biomed. Circuits Syst.*, vol. 9, no. 5, pp. 620–630, Oct. 2015.
- [33] Y. Nam, B. Koo, A. Cichocki, and S. Choi, "GOM-Face: GKP, EOG, and EMG-based multimodal interface with application to humanoid robot control," *IEEE Trans. Biomed. Eng.*, vol. 61, no. 2, pp. 453–462, Feb. 2014.
- [34] R. D. Flint *et al.*, "Extracting kinetic information from human motor cortical signals," *Neuroimage*, vol. 101, pp. 695–703, Nov. 2014.
- [35] N. Celadon, S. Došen, I. Binder, P. Ariano, and D. Farina, "Proportional estimation of finger movements from high-density surface electromyography," *J. Neuroeng. Rehabil.*, vol. 13, no. 1, p. 73, Aug. 2016.
- [36] Z. Li, B. Wang, F. Sun, C. Yang, Q. Xie, and W. Zhang, "SEMG-based joint force control for an upper-limb power-assist exoskeleton robot," *IEEE J. Biomed. Health Inform.*, vol. 18, no. 3, pp. 1043–1050, May 2014.
- [37] T. Lenzi, S. M. M. D. Rossi, N. Vitiello, and M. C. Carrozza, "Intention-based EMG control for powered exoskeletons," *IEEE Trans. Biomed. Eng.*, vol. 59, no. 8, pp. 2180–2190, Aug. 2012.
- [38] H. M. Shen, L. Hu, K. M. Lee, and X. Fu, "Multi-motion robots control based on bioelectric signals from single-channel dry electrode," *Proc. Inst. Mech. Eng. H*, vol. 229, no. 2, pp. 124–136, Feb. 2015.
- [39] T. F. Bastos-Filho *et al.*, "Towards a new modality-independent interface for a robotic wheelchair," *IEEE Trans. Neural Syst. Rehabil. Eng.*, vol. 22, no. 3, pp. 567–584, May 2014.
- [40] K. Bouyarmane, J. Vaillant, N. Sugimoto, F. Keith, J. Furukawa, and J. Morimoto, "Brain-machine interfacing control of whole-body humanoid motion," *Frontiers Syst. Neurosci.*, vol. 8, p. 138, Aug. 2014.
- [41] C. S. Chung, H. Wang, and R. A. Cooper, "Autonomous function of wheelchair-mounted robotic manipulators to perform daily activities," in *Proc. IEEE Int. Conf. Rehabil. Robot. (ICORR)*, Seattle, WA, USA, Jun. 2013, pp. 1–6.
- [42] A. C. Lopes, U. Nunes, L. Vaz, and L. Vaz, "Assisted navigation based on shared-control, using discrete and sparse human-machine interfaces," in *Proc. IEEE Eng. Med. Biol. Annu. Int. Conf.*, Buenos Aires, Argentina, Sep. 2010, pp. 471–474.
- [43] L. Pérez, I. Rodríguez, N. Rodríguez, R. Usamentiaga, and D. F. García, "Robot guidance using machine vision techniques in industrial environments: A comparative review," *Sensors*, vol. 16, no. 3, p. 335, Mar. 2016.
- [44] J. Zhang, L. Zhuang, Y. Wang, Y. Zhou, Y. Meng, and G. Hua, "An egocentric vision based assistive co-robot," in *Proc. IEEE Int. Conf. Rehabil. Robot. (ICORR)*, Seattle, WA, USA, Jun. 2013, pp. 1–7.
- [45] L. Minati, A. Nigri, C. Rosazza, and M. G. Bruzzone, "Thoughts turned into high-level commands: Proof-of-concept study of a vision-guided robot arm driven by functional MRI (fMRI) signals," *Med. Eng. Phys.*, vol. 34, no. 5, pp. 650–658, Jun. 2012.
- [46] A. Finke, A. Knoblauch, H. Koesling, and H. Ritter, "A hybrid brain interface for a humanoid robot assistant," in *Proc. IEEE Eng. Med. Biol. Soc. Annu. Int. Conf.*, Boston, MA, USA, Sep. 2011, pp. 7421–7424.
- [47] *Publicly Available Data*, accessed on Sep. 22, 2016. [Online]. Available: http://www.lminati.it/listing/2016/b/suppl_mat.tar.gz
- [48] A. Rowe, A. Goode, D. Goel, and I. Nourbakhsh, "CMUCam3: An open programmable embedded vision sensor," Carnegie Mellon Robot. Inst. Pittsburgh, Pittsburgh, PA, USA, Techn. Rep., RI-TR-07-13, May 2007.
- [49] G. J. Braun and M. D. Fairchild, "Image lightness rescaling using sigmoidal contrast enhancement functions," *J. Electron. Imag.*, vol. 8, no. 4, pp. 380–393, Oct. 1999.
- [50] P. K. Artempiadis and K. J. Kyriakopoulos, "An EMG-based robot control scheme robust to time-varying EMG signal features," *IEEE Trans. Inf. Technol. Biomed.*, vol. 14, no. 3, pp. 582–588, May 2010.
- [51] N. M. López, F. di Sciascio, C. M. Soria, and M. E. Valentiniuzzi, "Robust EMG sensing system based on data fusion for myoelectric control of a robotic arm," *Biomed. Eng. Online*, vol. 8, p. 5, Feb. 2009.
- [52] J. R. Wolpaw, "Brain-computer interfaces as new brain output pathways," *J. Physiol.*, vol. 579, pp. 613–619, Mar. 2007.
- [53] R. Barea, L. Boquete, M. Mazo, and E. Lopez, "System for assisted mobility using eye movements based on electrooculography," *IEEE Trans. Neural Syst. Rehabil. Eng.*, vol. 10, no. 4, pp. 209–218, Dec. 2002.

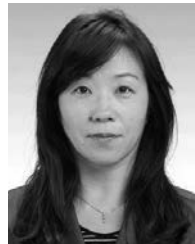
- [54] D. P. McMullen *et al.*, "Demonstration of a semi-autonomous hybrid brain-machine interface using human intracranial EEG, eye tracking, and computer vision to control a robotic upper limb prosthetic," *IEEE Trans. Neural Syst. Rehabil. Eng.*, vol. 22, no. 4, pp. 784–796, Jul. 2014.
- [55] R. Maskeliunas, R. Damasevicius, I. Martisius, and M. Vasiljevas, "Consumer-grade EEG devices: Are they usable for control tasks?" *PeerJ*, vol. 4, p. e1746, Mar. 2016.
- [56] B. Amanpour and A. Erfanian, "Classification of brain signals associated with imagination of hand grasping, opening and reaching by means of wavelet-based common spatial pattern and mutual information," in *Proc. IEEE 35th Annu. Int. Conf. Eng. Med. Biol. Soc. (EMBC)*, Osaka, Japan, Jul. 2013, pp. 2224–2227.
- [57] A. K. Mohamed, T. Marwala, and L. R. John, "Single-trial EEG discrimination between wrist and finger movement imagery and execution in a sensorimotor BCI," in *Proc. IEEE Eng. Med. Biol. Soc. Annu. Int. Conf.*, Boston, MA, USA, Sep. 2011, pp. 6289–6293.
- [58] V. Morash, O. Bai, S. Furlani, P. Lin, and M. Hallett, "Classifying EEG signals preceding right hand, left hand, tongue, and right foot movements and motor imageries," *Clin. Neurophysiol.*, vol. 119, no. 11, pp. 2570–2578, Nov. 2008.
- [59] A. Y. Paek, A. Gailey, P. Parikh, M. Santello, and J. Contreras-Vidal, "Predicting hand forces from scalp electroencephalography during isometric force production and object grasping," in *Proc. IEEE 37th Annu. Int. Conf. Eng. Med. Biol. Soc. (EMBC)*, Milan, Italy, Aug. 2015, pp. 7570–7573.
- [60] K. Nakayashiki, M. Saeki, Y. Takata, Y. Hayashi, and T. Kondo, "Modulation of event-related desynchronization during kinematic and kinetic hand movements," *J. Neuroeng. Rehabil.*, vol. 11, p. 90, May 2014.
- [61] M. Zaepffel, R. Trachel, B. E. Kilavik, and T. Brochier, "Modulations of EEG beta power during planning and execution of grasping movements," *PLoS ONE*, vol. 8, no. 3, p. e60060, Mar. 2013.
- [62] C. S. Nam, Y. Jeon, K. J. Kim, I. Lee, and K. Park, "Movement imagery-related lateralization of event-related (de)synchronization (ERD/ERS): Motor-imagery duration effects," *Clin. Neurophysiol.*, vol. 122, no. 3, pp. 567–577, Mar. 2011.
- [63] G. Pfurtscheller and C. Neuper, "Future prospects of ERD/ERS in the context of brain-computer interface (BCI) developments," *Prog. Brain Res.*, vol. 159, pp. 433–437, 2006.
- [64] C. Neuper, M. Wörtz, and G. Pfurtscheller, "ERD/ERS patterns reflecting sensorimotor activation and deactivation," *Prog. Brain Res.*, vol. 159, pp. 211–222, Oct. 2006.
- [65] R. Al-Halimi and M. Moussa, "Complex tasks by users with upper-extremity disability using a 6-DOF robotic arm: A study," *IEEE Trans. Neural Syst. Rehabil. Eng.*, vol. PP, no. 99, pp. 1–1, Aug. 2016.
- [66] J. Schmidhuber, "Deep learning in neural networks: An overview," *Neural Netw.*, vol. 61, pp. 85–117, Jan. 2015.
- [67] R. Memisevic, "Learning to relate images," *IEEE Trans. Pattern Anal. Mach. Intell.*, vol. 35, no. 8, pp. 1829–1846, Aug. 2013.
- [68] B. J. Driessens, H. G. Evers, and J. A. van Woerden, "MANUS: A wheelchair-mounted rehabilitation robot," *Proc. Inst Mech. Eng. H*, vol. 215, no. 3, pp. 285–290, 2001.
- [69] P. Geethanjali, "Myoelectric control of prosthetic hands: State-of-the-art review," *Med. Devices (Auckl)*, vol. 9, pp. 247–255, Jul. 2016.
- [70] W. K. Song, W. J. Song, Y. Kim, and J. Kim, "Usability test of KNRC self-feeding robot," in *Proc. IEEE Int. Conf. Rehabil. Robot. (ICORR)*, Seattle, WA, USA, Jun. 2013, pp. 1–5.
- [71] R. Soyama, S. Ishii, and A. Fukase, "The development of meal-assistance robot 'my spoon,'" *Proc. 8th Int. Conf. Rehabil. Robot.*, Tokyo, Japan, 2003, pp. 88–91.
- [72] J. Yao, Z. Jiao, D. Ma, and L. Yan, "High-accuracy tracking control of hydraulic rotary actuators with modeling uncertainties," *IEEE/ASME Trans. Mechatronics*, vol. 19, no. 2, pp. 633–641, Apr. 2014.
- [73] Z. Chen, B. Yao, and Q. Wang, " μ -synthesis-based adaptive robust control of linear motor driven stages with high-frequency dynamics: A case study," *IEEE/ASME Trans. Mechatronics*, vol. 20, no. 3, pp. 1482–1490, Jun. 2015.
- [74] W. Sun, S. Tang, H. Gao, and J. Zhao, "Two time-scale tracking control of nonholonomic wheeled mobile robots," *IEEE Trans. Control Syst. Technol.*, vol. 24, no. 6, pp. 2059–2069, Nov. 2016.



LUDOVICO MINATI (M'00–SM'13) received the B.Sc. degree in IT and computing and the M.S. degree in Science from The Open University, Milton Keynes, U.K., in 2004 and 2006, respectively, the M.S. degree in applied cognitive neuroscience from the University of Westminster, London, U.K., in 2008, the B.S. degree in physical science and the M.S. degree in medical physics from The Open University in 2009, and the Ph.D. degree in Neuroscience from the Brighton and Sussex Medical School, Falmer, U.K., in 2012.

He has held research and consulting roles across private companies and public institutions including the Carlo Besta Neurological Institute, Milan, Italy, and the Brighton and Sussex Medical School, Falmer. He has (co-)authored over 100 articles, and five inventions. He is currently a Visiting Professor with the Complex Systems Theory Department, Institute of Nuclear Physics-Polish Academy of Sciences, Kraków, Poland, a Guest Fellow with the Center for Mind/Brain Sciences, University of Trento, Italy, and a Freelance Consultant. His research interests include nonlinear dynamical systems, chaotic oscillators, reconfigurable analog and digital computing, functional magnetic resonance imaging, advanced techniques for bio-signal analysis, brain machine/computer interfaces, and robotics.

He is a Chartered Engineer and a member of the Institute of Engineering and Technology, Stevenage, U.K., Chartered Physicist. He is a member of the Institute of Physics, London, U.K., and a Chartered Scientist and member of the Institute of Physics and Engineering in Medicine, York, U.K.



NATSUE YOSHIMURA received the M.S. degree from Tokyo Medical and Dental University, Japan, in 2006, and the Ph.D. degree from The University of Electro-communications, Japan, in 2009.

She was a Post-Doctoral Researcher with the Tokyo Institute of Technology from 2009 to 2010 and became an Assistant Professor. She has been an Associate Professor with the Institute of Innovative Research, Tokyo Institute of Technology, since 2015. She is also a Visiting Researcher with

Integrative Brain Imaging Center, National Center of Neurology and Psychiatry. Her research interests include brain machine/computer interfaces, brain activity information decoding relating to motor control, speech, and emotion, using noninvasive brain activity recording methods such as electroencephalography, and functional magnetic resonance imaging.

She is a member of the Society for Neuroscience, the Japan Neuroscience Society, and the Japanese Society for Medical and Biological Engineering.



YASUHARU KOIKE received the B.S., M.S., and Ph.D. degrees in engineering from the Tokyo Institute of Technology, Tokyo, Japan in 1987, 1989, and 1996.

From 1989 to 1998, he was with Toyota Motor Corporation. From 1991 to 1994, he transferred to the Advanced Tele-communications Research Human Information Processing Laboratories, Kyoto, Japan. In 1998, he moved to the Precision and Intelligence Laboratory, Tokyo Institute of Technology, Tokyo, Japan, where he is currently a Professor of the Institute of Innovative Research. He was a Researcher of the Precursory Research for Embryonic Science and Technology, Japan Science and Technology Corporation, from 2000 to 2004 and of CREST, JST, from 2004 to 2014.

His research interests include human motor control theory, human interface, brain machine interface and their applications. He is a member of the Society for Neuroscience, IEICE, VRSJ, and JNNS.